Shear velocity structure beneath the central United States from the inversion of Rayleigh wave phase velocities

Y. Geng[1], U. Basu[1], and C. A. Powell[1]

[1]Center for Earthquake Research and Information, University of Memphis, Tennessee, USA.

Corresponding author: Yu Geng (ygeng1@memphis.edu)

Key Points:

- We present a 3-D Vs model for the upper mantle in the central United States by inverting Rayleigh wave phase velocities.
- A low Vs anomaly is imaged below the Reelfoot Rift, which is the uppermost portion of a prominent LVZ in previous tomographic studies.
- Low Vs anomalies are found in the mantle below the Ste. Genevieve and Wabash Valley seismic zones.

Abstract

A three-dimensional shear velocity model for the crust and upper mantle beneath the central United States is presented by inverting Rayleigh wave phase velocities from 20s to 100s periods. These phase velocities were determined using regional and teleseismic earthquakes recorded by the Northern Embayment Lithospheric Experiment stations, the CERI New Madrid Seismic Network, the Earthscope Transportable Array, and the Ozark Illinois INdiana Kentucky Flexible Array. A low Vs anomaly is imaged in the mantle below the Reelfoot Rift, which is the uppermost portion of connected low-velocity zones dipping toward the southwest below the rift and to the northwest below the Illinois Basin. According to the analysis in previous tomographic studies using both Vp and Vs anomalies, the elevation of temperature and the enrichment of iron, water, and orthopyroxene contents are required factors to explain the reduced seismic velocities. These low-velocity zones are produced by silica-rich fluids rising from the stalled Farallon slab. Two weak zones characterized by low Vs are imaged below the Ste. Genevieve and the Wabash Valley seismic zones. The low-velocity, weak areas may be responsible for stress concentration and thus the generation of intraplate seismicity.

Plain Language Summary

We present a three-dimensional seismic velocity model for the northern Mississippi Embayment and southern Illinois Basin derived from seismic waves that travel along the surface of the earth. These surface waves consist of many wavelengths. Short wavelengths travel through shallow parts of the crust while long wavelengths penetrate deeper into the earth, allowing construction of a velocity model from the near surface to a depth of 150 km. Our study utilizes seismic tomography to map velocity anomalies, much like tomography is used to produce images of the human body. We find anomalously high velocities in the crust below the three active seismic

zones in the area, the New Madrid, Wabash Valley, and Ste. Genevieve seismic zones. Anomalously low velocities underlie the seismic zones at greater depths below the crust. The slow velocities imply that the rocks are weak, and their presence may be concentrating stress in the seismic zones. We find anomalously low velocities below the crust in the northern Mississippi Embayment that extend to the bottom of the model. This low-velocity region has been detected in previous studies and is attributed to the effects of fluids coming from a trapped slab fragment at depths below 400 km.

1 Introduction

The central United States (CUS) has several active intraplate seismic zones lying near to each other: the New Madrid Seismic Zone (NMSZ), the Ste. Genevieve Seismic Zone (SGSZ) and the Wabash Valley Seismic Zone (WVSZ) (Figure 1). The Reelfoot Rift hosts the NMSZ and is acting as a zone of weakness where intraplate deformation concentrates (e.g., Csontos et al., 2008; Tavakoli et al., 2010; Thomas & Powell, 2017). Three major magnitude earthquakes were produced in the NMSZ from 1811 to 1812 (Johnston & Schweig, 1996). To the north of the NMSZ, the SGSZ and the WVSZ possess the same potential for creating large earthquakes. Due to the slow deformation rates at intraplate fault zones, intraplate earthquakes occur at a lower frequency than interplate earthquakes. Several attempts have been made to explain the origin of the NMSZ, but why the zone exists remains enigmatic. Examples include stress transfer from a weak lower crustal zone embedded within the elastic lithosphere (Kenner & Segall, 2000), a high compressional stress level due to density changes across a lateral transition in the upper mantle (Thybo et al., 2000), and high differential stress produced by a mafic body located in the deep crust beneath the NMSZ (e.g., Grana & Richardson, 1996; Pollitz et al., 2001). Recent studies

attempted to link the occurrence of intraplate earthquakes to stress concentration in the upper crust produced by changes in lithospheric thickness and the presence of anomalously low velocity in the upper mantle (e.g., Biryol et al., 2016; Zhan et al., 2016). Biryol et al. (2016) hypothesized that tectonic inheritance involving a sharp change in lithosphere thickness as well upwelling asthenosphere might control the ongoing activity of the region. Zhan et al. (2016) found that low mantle velocities underneath the NMSZ play a pivotal role in increasing the differential stress in the layers above. Elevated stresses are enabled by the strong lower crust in this region, and subsequently, earthquakes are triggered by reactivated pre-existing faults within the base of ancient rifts.

Shear wave velocities in the crust and upper mantle reflect changes in the thermal, mineralogical, and compositional properties of the lithosphere. The surface wave and shear wave velocity structure of the CUS is presented in many regional and global studies (e.g., Godey et al., 2003; Van der Lee, 2002; Van Der Lee & Frederiksen, 2005; Van der Lee & Nolet, 1997). A strong velocity contrast between low velocities in the western North America and high velocities beneath the North American craton is a first order observation found in many studies (i.e., Godey et al., 2003; Porritt et al., 2014; Shen & Ritzwoller, 2016). An anomalously slow velocity area was imaged in the uppermost mantle underneath the Illinois Basin (Van der Lee, 2002; Van Der Lee & Frederiksen, 2005). The model was enhanced in the study by Bedle and van der Lee (2006) where it was suggested that this area may reflect the presence of oceanic crust or hydrous mantle associated with a fossilized flat slab. Shen et al. (2013) revealed the significance of Precambrian sutures in the tectonic evolution of the CUS from Rayleigh wave phase velocities across the Midcontinent Rift and surrounding regions. Recently, studies using the Northern Embayment Lithosphere Experiment (NELE), the Ozarks-Illinois-INdiana-Kentucky Flexible

Array (OIINK), and the EarthScope transportable array (TA) deployments revealed a low-velocity zone (LVZ) in the upper mantle below the Mississippi Embayment (ME) (e.g., Nyamwandha et al., 2016; Pollitz & Mooney, 2014). The highest resolution image of the LVZ below the NMSZ is provided by Nyamwandha et al. (2016), which shows the LVZ dips to the southwest and extends to a depth of at least 250 km. Another two low-velocity anomalies at depths ~200 to 400 km below the Illinois Basin are imaged by Geng et al. (2020). The slow velocities form a northwest dipping zone and indicate the presence of a large igneous province.

In addition, studies involving Pn velocities and uppermost mantle anisotropy in the central and eastern United States (CEUS) provided information about tectonic processes. Zhang et al. (2009) constructed a Pn tomographic model that revealed high-velocity anomalies in the uppermost mantle below the NMSZ and southern Illinois Basin. Inconsistency between Pn fast axes and SKS splitting orientations in the CEUS observed by Buehler and Shearer (2017) suggest significant vertical changes in anisotropy in the upper mantle. Using Pn arrivals recorded by TA stations, Basu and Powell (2019) found a correlation between Pn velocity variations and Moho depth variations in the southern Illinois Basin as well as a curious circular anisotropy pattern centered on the NMSZ. The SKS splitting study by Nyamwandha and Powell (2016) for the CUS indicated consistency between the direction of absolute plate motion (APM) and upper mantle anisotropy except in the Mississippi Embayment; within the Embayment, large and systematic deviations from the APM directions were attributed to relic lithospheric fabrics formed during past tectonic events.

In this paper, we investigate shear velocity structure for the CUS by inverting Rayleigh wave phase velocities obtained by Basu (2019). The combined dataset from the NELE stations, the OIINK array, and the TA provide a high-resolution image. The study aims to provide insight

into the connections between the Reelfoot Rift and the Illinois Basin. The study will also reveal any relationship between mantle structure and the intraplate seismicity. We are motivated by these outstanding questions in the CUS continental tectonics: (1) How could the structures below the Illinois Basin be related to structures below the northern Reelfoot Rift? Are the two regions distinctly different? (2) What are the possible contributions of mantle velocity structures to the seismic zones?

2 Tectonic setting

2.1 The North American Craton

The CUS is located within the North American craton – a large and coherent portion of the North American continental crust that has maintained long-term stability (Whitmeyer & Karlstrom, 2007). The craton consists of the Archean Canadian Shield and the cratonic platform, where the Precambrian basement complex is overlain by minimally deformed sedimentary strata (Yang et al., 2017). The basement below our study area is part of the extensive Proterozoic Granite-Rhyolite province. The Grenville Front, formed by the assembly of the supercontinent Rodinia in the late Mesoproterozoic, is typically considered as the southeastern margin of the North American midcontinent. The geological background of intraplate seismic zones is closely related to the evolution of the North American continent, in that the Reelfoot Rift and the Rough Creek Graben were formed during the breakup of Rodinia in the Late Proterozoic and Early Cambrian (Figure 1). The assembly of supercontinent Pangea created a compressional environment, in which intracratonic rifts were reactivated during the late Paleozoic (e.g., Thomas, 2014).

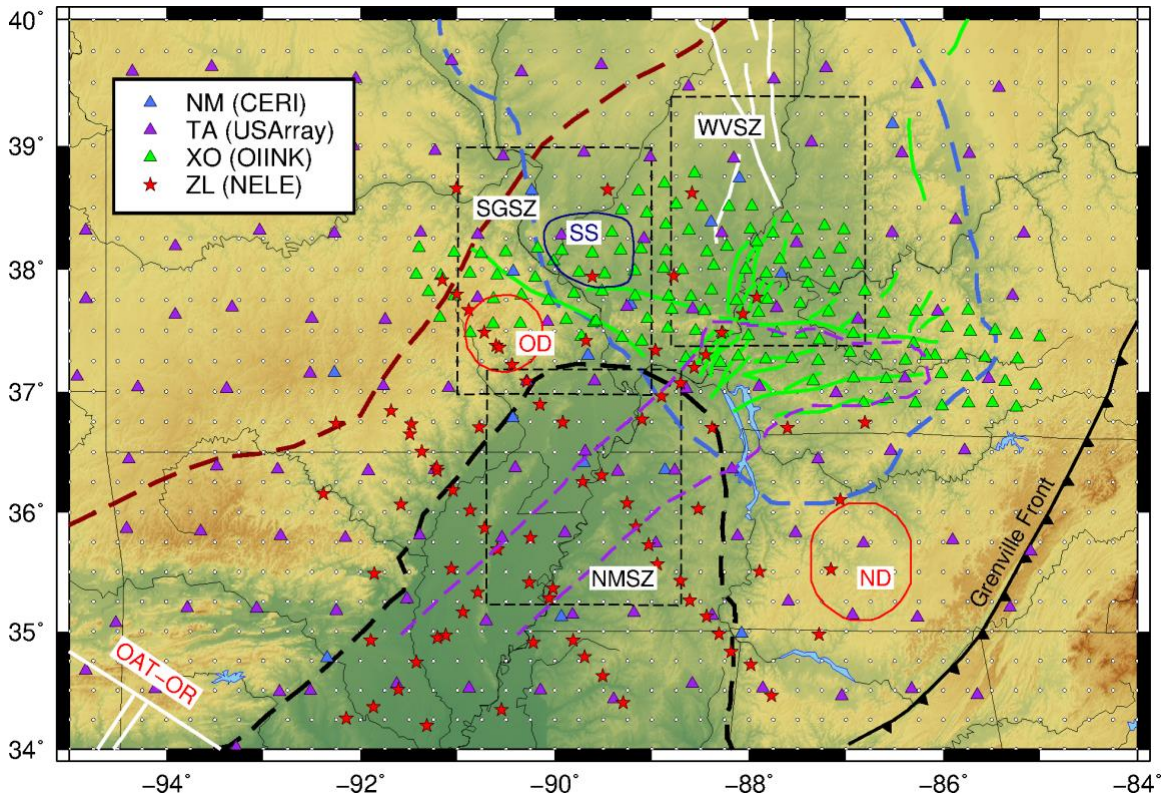

Figure 1. 348 NELE, CERI, OIINK, and TA stations utilized in the Basu (2019) study to obtain Rayleigh wave phase velocities. SS, the Sparta Shelf; OD, the Ozark Dome; ND, the Nashville Dome; OAT, the Oklahoma-Alabama Transform; OR, the Ouachita Rift; NMSZ, the New Madrid Seismic Zone; SGSZ, the Ste. Genevieve Seismic Zone; WVSZ, the Wabash Valley Seismic Zone. A dashed line in dark red represents the Nd line. Fault traces and fold systems are delineated with green solid lines and white solid lines, respectively. Boundaries of the Illinois Basin, the Mississippi Embayment, and the Reelfoot Rift are marked with dashed lines in blue, black, and purple, respectively. Grid nodes used to present the phase velocity maps by Basu (2019) are denoted with empty dots.

2.2 Intraplate seismic zones

The Wabash Valley fault zone is composed of faults trending southwest-northeast. The faults originate near the junction of the Rough Creek and Cottage Grove faults (Brazitis & Conder, 2016) and trend parallel to the portion of the Wabash River between Illinois and Indiana (Cox & Van Arsdale, 2002). The northern WVSZ is connected with the La Salle anticlinal belt – an anticline that is geologically complex and consists of reverse faults (McBride, 1997) (white lines in Figure 1).

The earliest documented faulting in the Wabash Valley fault zone occurred in the Cambrian. Major faulting ended after the Pennsylvanian, and minor faulting possibly continued into the Pleistocene (Fraser et al., 1997) with most of the faults characterized as high-angle normal faults (Bristol & Treworgy, 1979). Paleoseismic data indicate that several events greater than magnitude 6.0 occurred in the last few thousand years (Obermeier, 1998). The WVSZ is still seismically active; there have been three earthquakes of magnitude 5.0 or higher in the last 50 years.

The SGSZ lies to the northeast of the Ozark Dome and along the western edge of the Illinois Basin. It is associated with Ste. Genevieve fault zone (Marshak & Paulsen, 1996; Yang et al., 2014) and has a connection with the reactivation of the Reelfoot Rift (Yang et al., 2014). The fault zone consists of NW-SE trending faults parallel to the Mississippi River and is the boundary between the Illinois Basin and the Ozark Dome (Marshak et al., 2017). The earliest faulting occurred in the Middle Devonian. The current seismic activity in the SGSZ is dominated by strike-slip mechanisms under horizontal compressive stresses (Yang et al., 2014).

2.3 The Illinois Basin

Intracratonic basins are sedimentary basins within the stable and cratonic interiors of continents. The Illinois Basin and the Michigan Basin in the North America are examples of such basins. The Nd line (Figure 1) goes through the northern part of the Illinois Basin and splits older crust in the NW from younger crust in the SE (Bickford et al., 2015).

Usually, the Illinois Basin is interpreted as a rift basin formed in the late Proterozoic (Braile et al., 1986; Keller et al., 1983), concurrent with the breakup of Rodinia. The oval shape of the basin can be attributed to an extension in the Early Permian due to the breaking of Pangaea; the uplift of the Pascola Arch at the southern edge of the basin was created in the same process (McKeown et al., 1990). Nevertheless, evidence from sequence stratigraphy (e.g., Pratt et al., 1992) and reflection profiles (e.g., McBride and Kolata, 1999) indicate that the Reelfoot Rift is not the initial mechanism that formed the Illinois Basin. Localized subsidence and volcanic accumulation before the deposition of Cambrian layers suggest that the Illinois Basin had been operating as a sedimentary basin (McBride and Kolata, 1999). McBride et al. (2003) proposed a two-episode mechanism that formed the Illinois Basin: firstly, a Proterozoic basin overlies a rhyolitic caldera complex; and secondly, the deposition center shifted southward during the Reelfoot Rift extension.

More recently, a receiver function study (Yang et al., 2017) found a thick crust below the central and southern portion of the basin; the crust below the Sparta Shelf is ~15 km thicker than that below the Ozark Dome. The crustal thickness variation occurred prior to the formation of the Illinois Basin, elaborated with several hypothesis (delamination, underthrusting, and magmatic underplating) by Yang et al. (2017).

3 Preparation

3.1 Data and method

This study is based on the Rayleigh wave phase velocity maps at eight periods between 20 sec and 100 sec from Basu (2019), as summarized in Table 1. Azimuthal anisotropy was determined simultaneously with isotropic phase velocities using the method by Yao et al. (2010) – a technique based on the regionalization method of Montagner (1986) and the generalized inversion scheme of Tarantola and Valette (1982). Some resolution tests were conducted to validate the reliability of the models, as presented in Supporting Information **Text S1**. The tradeoff between azimuthal anisotropy and heterogeneity was minimal and azimuthal anisotropy was not considered in this study.

Table 1. Rayleigh wave phase velocities between 20 sec and 100 sec measured by combining data from all the grid nodes[a].

Period [s]	Nobs	$\overline{C_0}$ [km/s]	σ_d [km/s]
20	6540	3.61	0.064
30	9640	3.85	0.056
40	10569	3.99	0.055
50	10442	4.06	0.067
60	10358	4.10	0.068
75	9593	4.14	0.084
90	8489	4.16	0.094
100	7877	4.19	0.100

[a]Note: Nobs – data count; $\overline{C_0}$ – averaged phase velocity; σ_d – standard deviation.

The study area covers the northern Mississippi Embayment and the southern Illinois Basin (Figure 1) and is parameterized into 49 grid nodes in longitude and 29 grid nodes in latitude spaced at 0.25°. To determine the most detailed phase velocity of the region to date, the Basu (2019) study used the combined dataset recorded by 119 TA stations, 84 NELE stations, 15 CERI permanent network stations, and 130 OIINK stations over a five-year period (2011-2015). The dataset consists of 104 regional and teleseismic events (Figure 2) with magnitudes ≥5.0 and epicentral distances 5°-120° (measured from the center of the northern ME). A two-station method (Satô, 1958) was applied to calculate fundamental mode Rayleigh wave phase velocities for two-station pairs. The grid nodes extend beyond the area covered by the selected stations to absorb travel time anomalies outside of the array area.

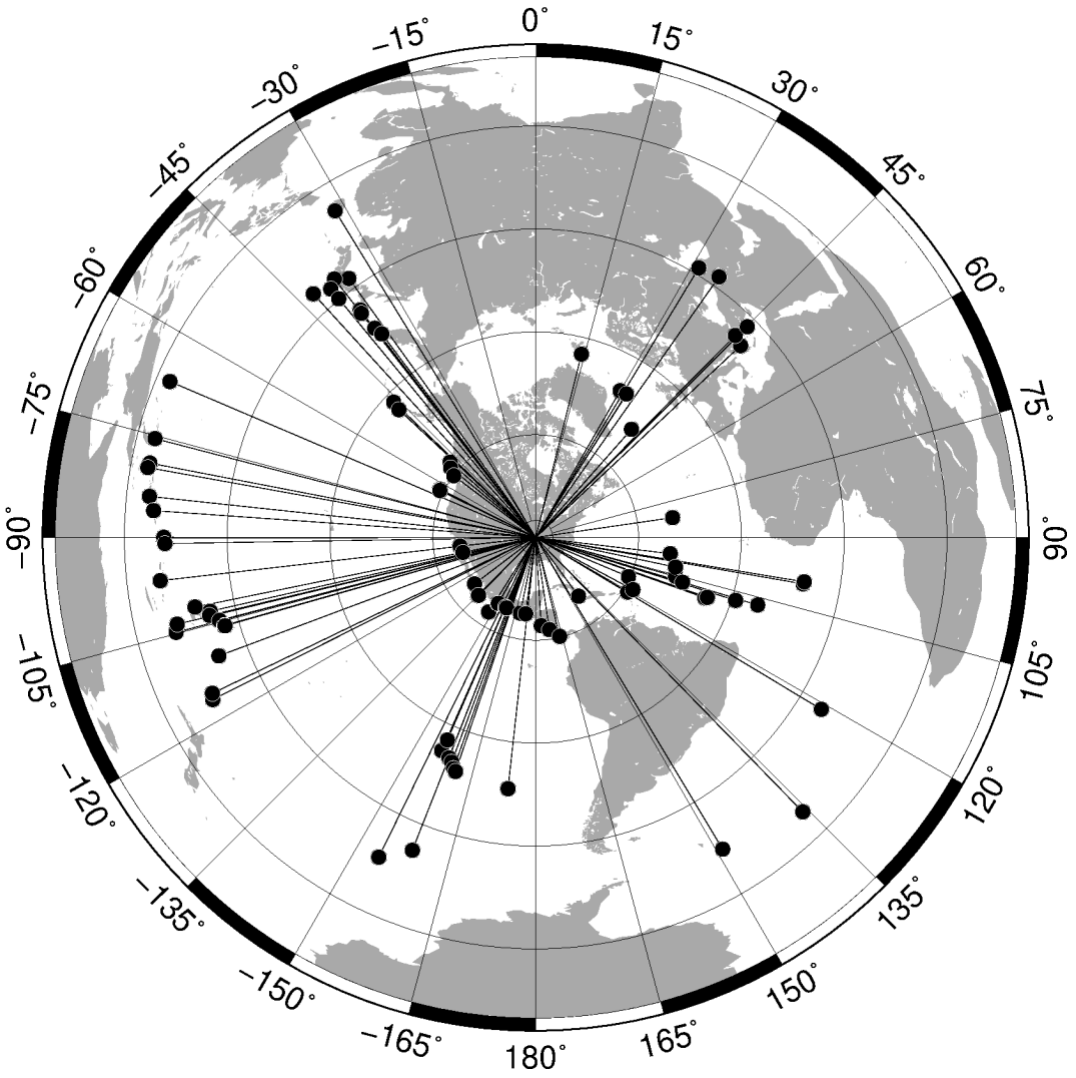

Figure 2. The azimuthal distribution and ray paths of 104 regional and teleseismic events with magnitudes ≥5.0 and epicentral distances 5°-120° (measured from the center of the northern Mississippi Embayment), from Basu (2019). They were selected over a period of five years (from 2011 to 2015).

The NELE stations were deployed in two time periods from September 2011 to October 2013 and from July 2013 to June 2015. The average spacing of the NELE stations is ~20 km (Nyamwandha et al., 2016). The OIINK Array, spaced at ~25 km, was divided into three

219 deployment phases that migrated from west to east. They were operated in July 2011 to June
220 2012 in the first phase, from June 2012 to the late 2013 in the second phase, and from August
221 2013 to October 2015 in the final phase (Chen et al., 2016). Compared to previous studies that
222 used only TA stations, the availability of NELE and OIINK stations will provide a higher
223 resolution image based on surface waves for the uppermost mantle below the CUS.

224 The averaged phase velocities over the study area vary between 3.61 km/s at 20 sec and
225 4.19 km/s at 100 sec, comparable to the values obtained in previous studies involving the CUS
226 (Chen et al., 2016; Shen et al., 2013). The phase velocities increase with periods up to 50 sec,
227 after which the slope of the curve becomes gentle (Figure 3), indicating that velocities with
228 periods greater than 50 sec are less sensitive to structures in the crust than the mantle (Shen &
229 Ritzwoller, 2016). A dispersion curve is obtained at each grid node by extracting Rayleigh wave
230 phase velocities at all the periods. The dispersion curve was inverted for a 1-D shear velocity
231 (Vs) profile using the method developed by Herrmann (2013). The weight of each layer in the
232 velocity model is set such that velocities in the upper 50 km are allowed to change more than
233 velocities for deep structures during the inversion. Finally, the 1-D Vs profiles at all grid nodes
234 were joined to create the resultant 3-D shear velocity images.

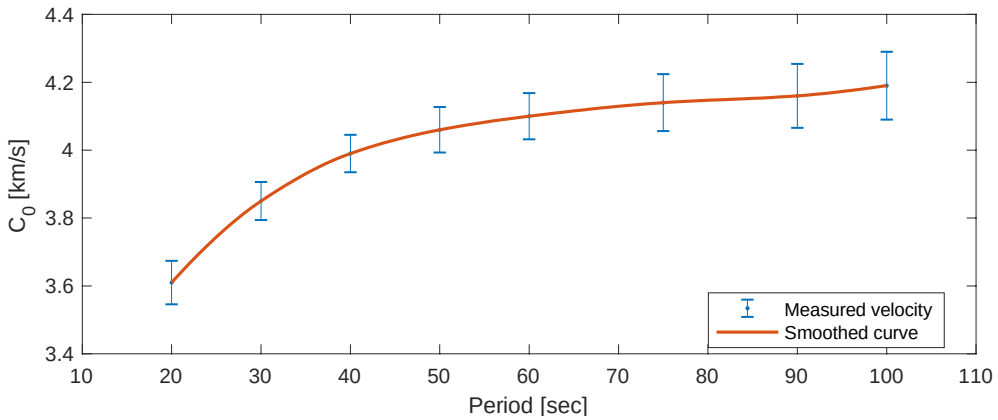

235

Figure 3. Averaged dispersion curve of Rayleigh wave phase velocities measured by combining data from all the grid nodes. The lengths of the blue bars are proportional to the magnitudes of standard errors.

3.2 Starting model

Two different 1-D Vs starting models are investigated. The first starting model was created by Herrmann (2013) and is a modification of the ak135-F velocity model (Kennett et al., 1995; Montagner & Kennett, 1996). Velocities in the upper 50 km of the ak135-F model were replaced with the velocity at 50 km, which yielded a constant velocity in the upper 50 km. This technique helps avoid sharp velocity discontinuities that would persist through the inversion and reduces the occurrences of low-velocity layers due to artifacts. The second starting model was used by Chen et al. (2016). This model uses the crustal velocities measured by Catchings (1999) and the mantle velocities of IASP91 (Kennett & Engdahl, 1991). To test the sensitivity of the resultant 1-D Vs profiles on the starting model, the two 1-D starting models were varied by ±0.2 km/s. When crustal velocities were perturbed, mantle velocities were fixed, and conversely, crustal velocities were fixed when mantle velocities were perturbed. The above modifications yield ten different starting models shown in Figure 4.

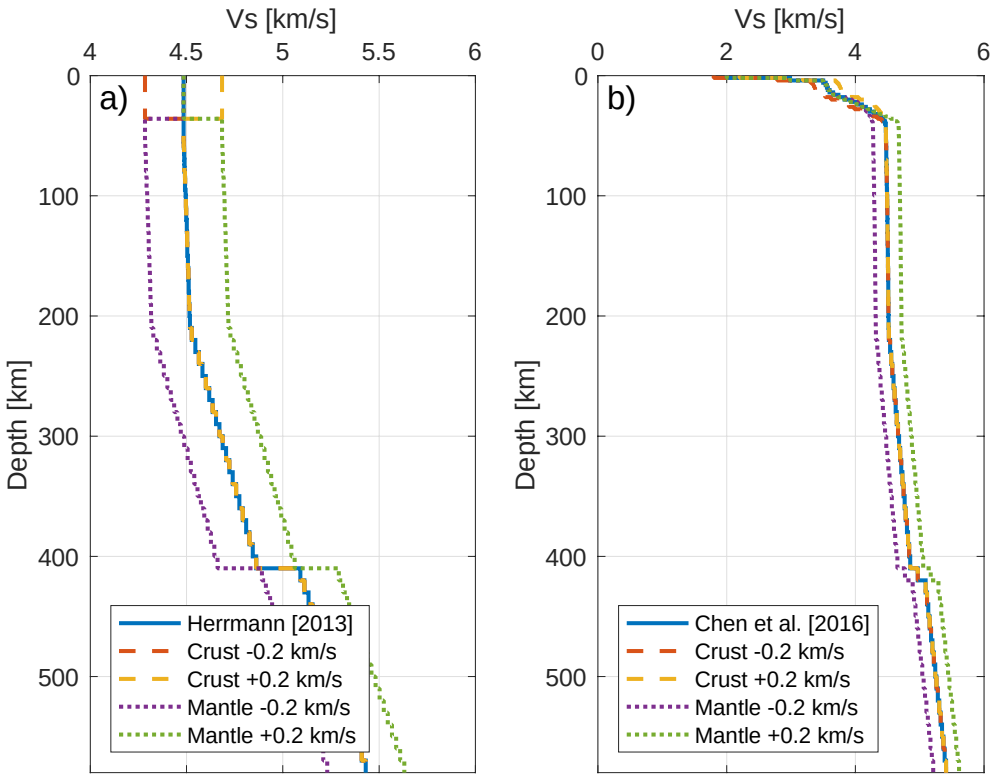

Figure 4. Starting models used to test the stability of shear velocity inversion: (a), the Herrmann (2013) model with variations of crustal or mantle velocities of ±0.2 km/s; (b), the Chen et al. (2016) model with variations of crustal or mantle velocities of ±0.2 km/s.

The influence of the starting model is demonstrated by showing the results at several locations. The first location, (38.25°N, 90.50°W), is in the SGSZ (Figure 5). For both the Herrmann (2013) and Chen et al. (2016) models, variations of either crustal velocities or mantle velocities in the starting model exert a more significant impact on crustal velocities than mantle velocities in the resultant Vs profiles (Figure 5b and 5c) (i.e., crustal velocities are more sensitive to the starting model than mantle velocities). The impact is most evident at depths of 25-40 km.

264 At depths 4-40 km, the velocities resolved using the Chen et al. (2016) model are larger than the
265 velocities resolved using the Herrmann (2013) model, and the opposite is true in the upper 4 km.

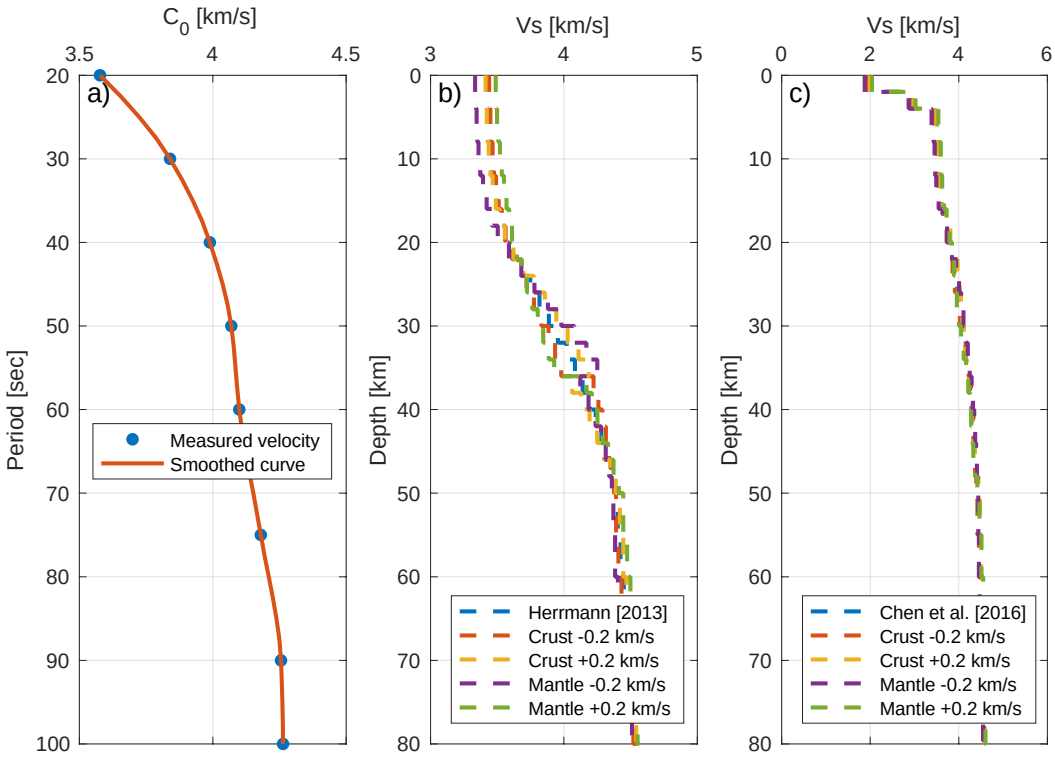

266

267 **Figure 5**. Impact of the starting model on the resultant Vs profile at (38.25°N, 90.50°W): (a) the
268 dispersion curve used to invert for Vs structure; (b) velocities resolved using the Herrmann
269 (2013) model with variations of crustal or mantle velocities; (c) velocities resolved using the
270 Chen et al. (2016) model with variations of crustal or mantle velocities.

271

272 Vs profiles for a location in the WVSZ (38.25°N, 88.00°W) are shown in Figure 6.
273 Similar to the observations for the SGSZ, velocity variations in the starting model exert a more
274 significant impact on crustal velocities than mantle velocities in the resultant Vs profiles (Figure
275 6b and Figure 6c). The most significant impact appears at depths of 20-40 km. A low-velocity

zone below the WVSZ is present at depths of 20-50 km. Although velocities resolved with the Herrmann (2013) model are lower than velocities resolved with the Chen et al. (2016) model within these depths, the two starting models produce consistent upper and lower bounds for the low-velocity zone. The above tests indicate that the starting model has little impact on the resolved mantle structures. We selected the Herrmann (2013) model to obtain the Vs images in this study. A more extensive discussion for selecting this model is presented in Supporting Information **Text S2**.

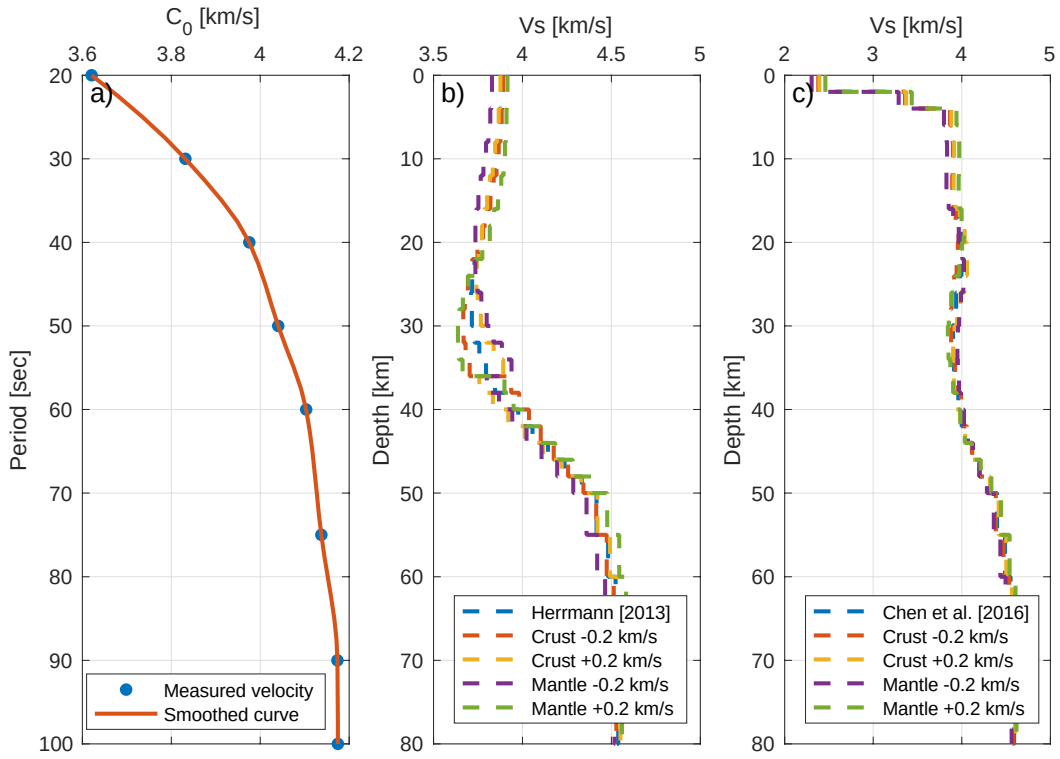

Figure 6. Impact of the starting model on the resultant Vs profile at (38.25°N, 88.00°W): (a) the dispersion curve used to invert for Vs structure; (b) velocities resolved using the Herrmann

(2013) model with variations of crustal or mantle velocities; (c) velocities resolved using the Chen et al. (2016) model with variations of crustal or mantle velocities.

4 Results

4.1 Phase velocity maps

Isotropic phase velocity maps are presented in Figure 7. At periods of 20-30s, Rayleigh wave phase velocities agree with previous work for the mid and lower crust by Chen et al. (2016). At 20s in both studies, a broad area of high velocities (labeled A) is present underneath most of the upper ME and below the Ozark uplift (Figure 7a). Unlike the Chen et al. (2016) results, the high velocities in our solution extend below the WVSZ. A pronounced low-velocity region (labeled B) is present in western Arkansas near the southern edge of our map. The Chen et al. (2016) map only extends over a small portion of the velocity low, but the same feature was identified by Liang and Langston (2009) at the same period in an analysis of Rayleigh wave group velocities. The low velocities coincide with the intersection of the Oklahoma-Alabama transform fault and the Ouachita Rift (OAT-OR). This is the location of a very negative Bouguer gravity anomaly, suggesting the presence of deeply buried, sedimentary rocks (Kruger & Keller, 1986; Thomas, 2014). At a period of 30s (Figure 7b), the Reelfoot Rift is flanked to the northwest (NW) and southeast (SE) by regions of high phase velocities (labeled C).

The phase velocity maps at 40s and longer periods are most sensitive to structure in the upper mantle (Shen & Ritzwoller, 2016). At a period of 50s (Figure 7d), several slow regions characterize the Reelfoot Rift (labeled D), and the Illinois Basin is surrounded by high velocities (labeled E). The same pattern of high and low velocities is present in the 60s period map (Figure

7e). High velocities along the SW edge of the Illinois Basin persist in the 75, 90, and 100s phase velocity maps. Several slow (labeled F) and fast (labeled G) areas within the interior of the Illinois Basin are identified in the 75, 90 and 100s period maps. A slow region (labeled H) is present at a location corresponding to the southernmost Illinois Basin and the western end of the Rough Creek Graben at 75-100s periods.

The average to low velocity pattern below the Reelfoot Rift and high velocities to the NW and SE of the rift persists at periods of 40s to 100s. The same high- and low-velocity pattern for the Reelfoot Rift is found in the 40s and higher phase velocity maps determined by Chen et al. (2016). Low velocities are present in our phase velocity maps below a latitude of 35°N at 40-100s periods. These low velocities are south of the phase velocity maps determined by Chen et al. (2016).

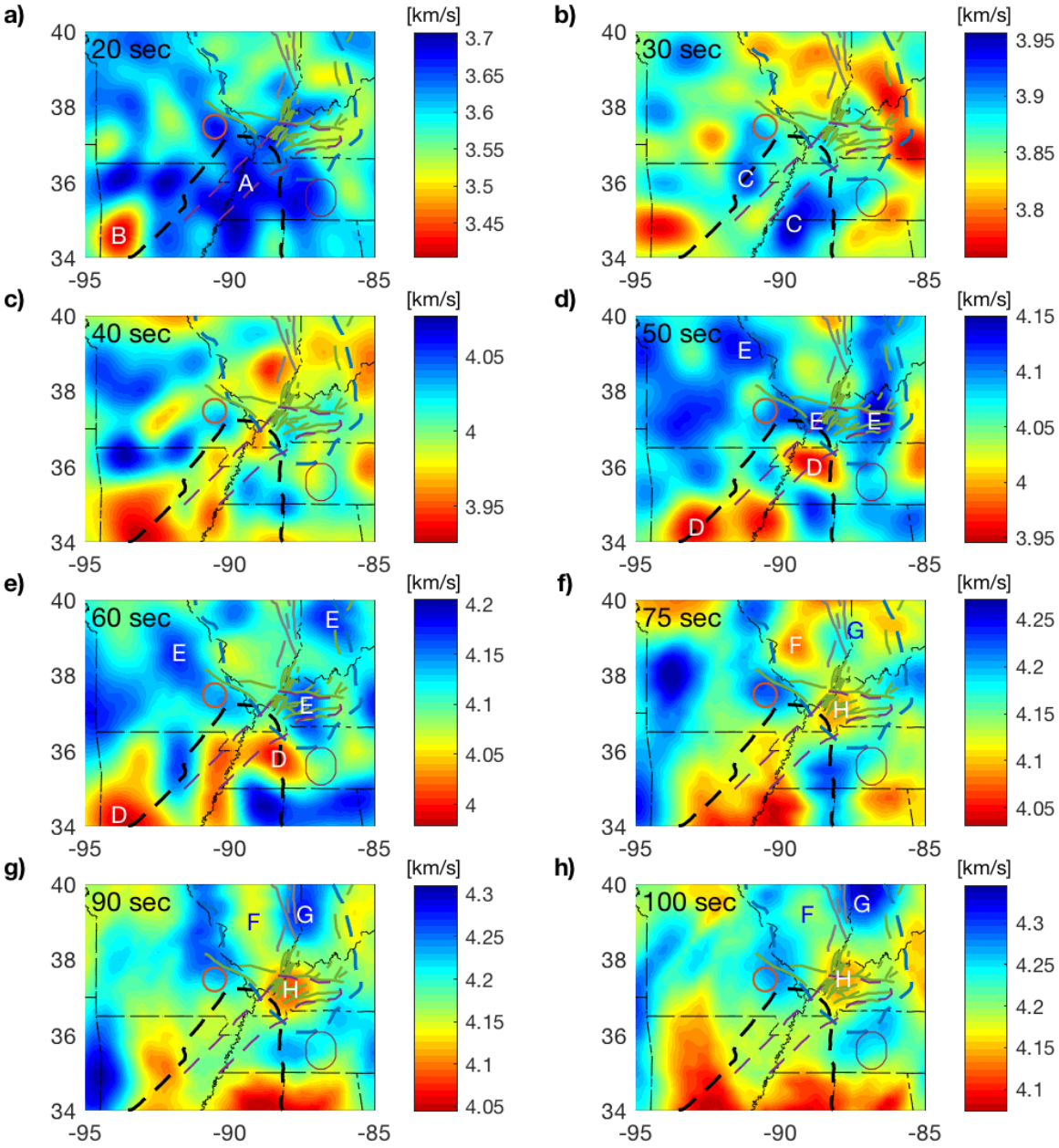

Figure 7. Isotropic phase velocity maps from simultaneous inversion for 20-100s periods. Fault traces and fold systems are delineated with solid green lines and solid gray lines, respectively. The Ozark Dome and the Nashville Dome are delineated with an orange circle and a dark red circle, respectively. A purple dashed line marks the boundary of the Reelfoot Rift. The

boundaries of the Illinois Basin and the Mississippi Embayment are delineated with a blue dashed line and a black dashed line, respectively.

4.2 Shear velocity inversion

The Vs images obtained using the Herrmann (2013) starting model are presented in Figure 8. Cross-section views are presented in three profiles (AA', BB', and CC') perpendicular to two profiles (DD' and EE') crossing the intraplate seismic zones (Figure 9). As a comparison, our results using the Chen et al. (2016) starting model are presented in Figure S2. There are only minor differences between the two solutions.

Velocities in the lower crust vary between 3.6 km/s and 4.7 km/s. High velocities in the 24 km slice make a three-arm pattern similar to the pattern found by Liang and Langston (2009) at 24 km based on ambient noise tomography. The only difference in the patterns is that high velocities do not extend as far NW along the margin of the Illinois Basin in our study. Our velocity high and low pattern at 36 km cannot be directly compared to the results obtained by Liang and Langston (2009) because a comparable depth slice is not presented. Our solution at 36 km appears to be a better-resolved version of the velocity pattern at 43 km in the Liang and Langston (2009) study. There is general agreement between our results and the shear wave velocity model determined by Chen et al. (2016) at 24 km and a stronger agreement at 36 km. In our study and the two previous studies, high-velocity anomalies are present in the lower crust below western Tennessee and along the southwest boundary of the Illinois Basin. These velocity anomalies are labeled I in Figure 8. Low velocities are present below the Ozark uplift and the Illinois Basin in our study (labeled J and K) and also in the studies by Liang and Langston (2009)

346 and Chen et al. (2016). Low velocities are found below the Rough Creek Graben in our results
347 (labeled L) and those of Liang and Langston (2009).

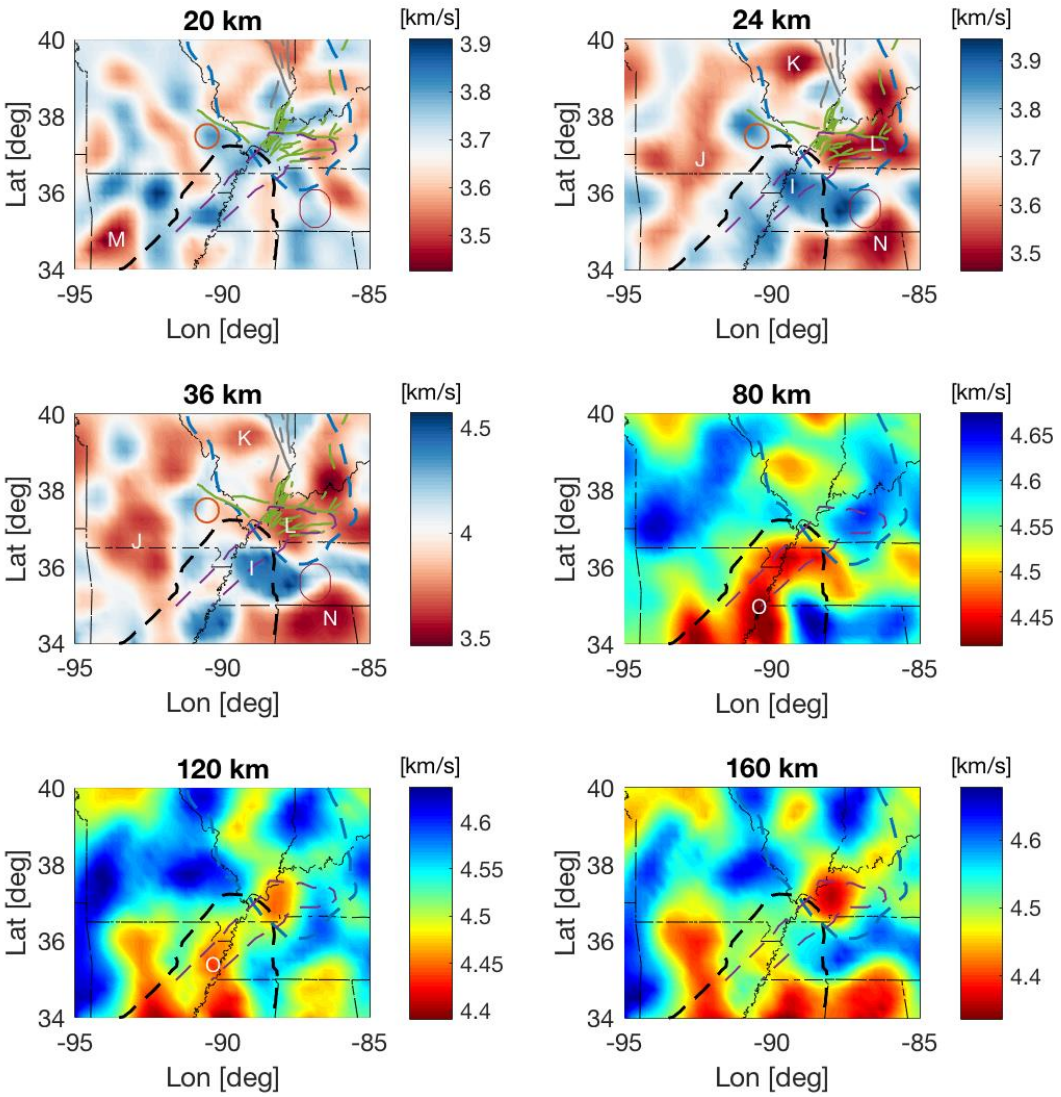

348

349 **Figure 8**. Horizontal slices of the 3-D Vs model created by joining all the 1-D profiles. Crustal
350 velocities and mantle velocities are presented using different color scales. Major geology
351 features are labeled with the same notations as those in Figure 7.

352

353 Velocities in the uppermost mantle (50~150 km depths) vary between 4.28 km/s and 4.92
354 km/s, which is relatively larger than the ranges of mantle velocities in the NA07 model by Bedle
355 and Van Der Lee (2009) and in the shear velocity model by Chen et al. (2016). Reduced
356 velocities in the mantle (labeled O) found in previous studies (e.g., Bedle and van der Lee, 2006;
357 Pollitz and Mooney, 2014; Chen et al., 2016; Nyamwandha et al., 2016) are present in cross-
358 section slices AA', BB', DD', and EE', and on the 80 km and 120 km slices of the map views. In
359 the Nyamwandha et al. (2016) study, this anomaly is located at 80-160 km depth, and the Vs
360 anomaly magnitude is −3% to −5% with respect to the IASP91 reference model. Chen et al.
361 (2016) determined the velocity reduction as about 7% compared to velocities outside of the
362 Reelfoot Rift; that is, the Vs anomaly below the rift is about 3.33% lower than the starting
363 model. In our model, the magnitude of this anomaly is ~3.8%. The upper bound of this low-
364 velocity area is at ~50 km depth, which agrees with the Nyamwandha et al. (2016) study.
365 Reduced resolution near the bottom of the model makes it difficult to tell the dipping direction of
366 anomaly O, but on cross-section DD', the feature seems dipping towards southwest and connects
367 with another larger low-velocity anomaly (labeled P) located at 150 km and deeper.

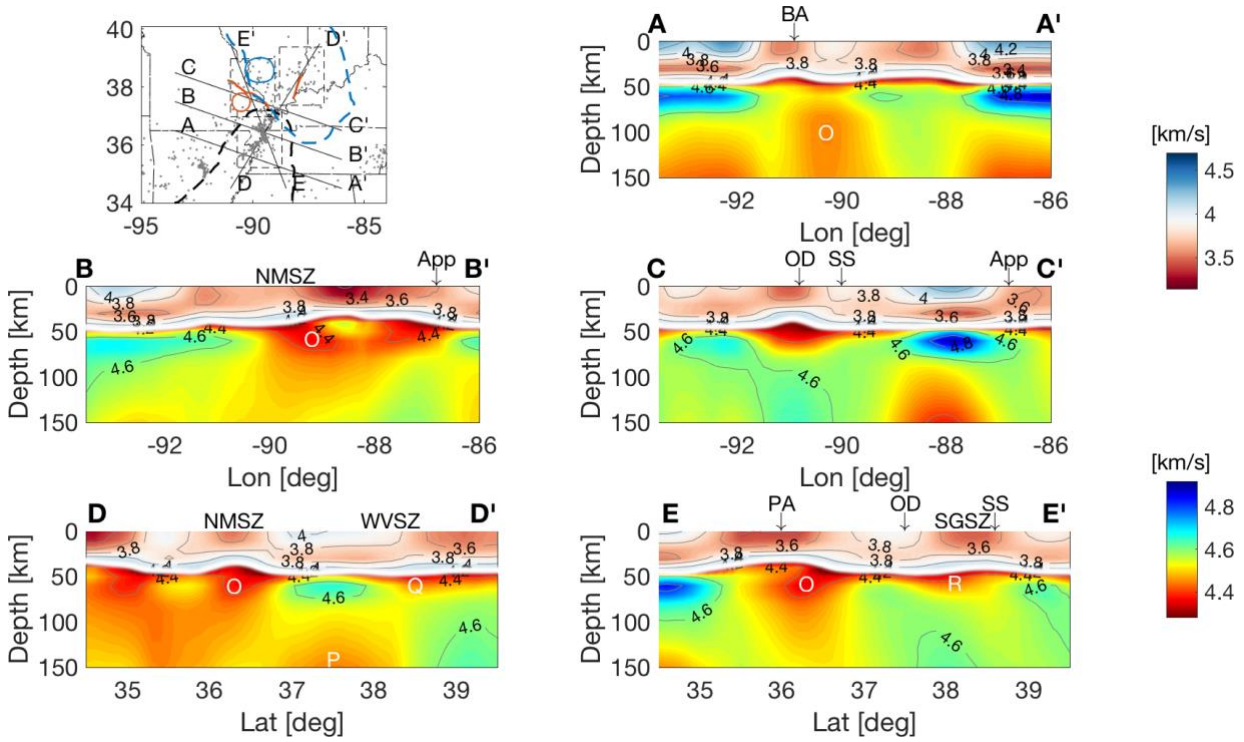

Figure 9. Vertical slices of the 3-D Vs model. The 4.2 km/s velocity contour is used to represent the Moho. Notations for major geology features: BA, the Blytheville Arch; OD, the Ozark Dome; SS, the Sparta Shelf; PA, the Pascola Arch; App, the Appalachian Basin; NMSZ, the New Madrid Seismic Zone; SGSZ, the Ste. Genevieve Seismic Zone; WVSZ, the Wabash Valley Seismic Zone. On the map view, the blue circle and the red circle mark the boundaries of the Sparta Shelf and the Ozark Dome, respectively; dashed rectangles mark the locations of intraplate seismic zones; fault zones are delineated with thick, orange lines.

We used the 4.2 km/s velocity contour (solid white lines in Figure 9) to represent the depth to Moho on each cross-section plot. Based on a comparison with the receiver function study by Yang et al. (2017), the contour is near the bottom of the crust in all cross-sections, and the value is close to the Vs value at the bottom of the crust in the AK-135 model (Kennett et al.,

1995; Montagner & Kennett, 1996). The majority of the Illinois Basin is dominated by a deep Moho with depths ~45 km, which is shown in cross-section DD' between 37°N and 39.5°N. A deepening of the Moho is observed near the eastern-most end (86°W) of cross-section BB'. The depression is possibly an effect of isostasy due to the elevated topography of the Appalachian thrust sheets and the presence of the Appalachian Basin. In the Yang et al. (2017) study, the Moho in the same location is slightly deeper than 50 km.

One of the most distinct features in the Yang et al. (2017) study is an abrupt transition of Moho depth from 45 km to ~60 km across the boundary between the Ozark Dome and the Sparta Shelf in the Illinois Basin. In our model, no significant variation of Moho depth between 37°N and 39°N is observed in cross-section EE' that goes through the NE edge of the Ozark Dome and the western edge of the Sparta Shelf (SS in Figure 9). We observe an elevation of the Moho (~40 km deep) below the Ozark Dome in cross-section CC'. Although the value is greater than the average depth of the Moho in continental North America (36.1 km), the Moho below the Ozark Dome is a localized feature and is surrounded by a deeper Moho at its flanks. To the southwest of the Sparta Shelf, the Pascola Arch is characterized by an elevated Moho surface with ~36.5 km depth, as indicated in cross-section EE'. In cross-section AA', the Blytheville Arch is characterized by a relatively shallow Moho with ~41 km depth.

5 Discussion

Our results reveal many features that agree with previous studies by Chen et al. (2016), Nyamwandha et al. (2016), and Geng et al. (2020). For example, an area dominated by low crustal Vs (labeled J in the map view in Figure 8) is present in southern Missouri and northern

Arkansas. The feature is more prominent in this study compared to that in Geng et al. (2020). This low-velocity anomaly coincides with a Bouguer gravity low that is interpreted as the Missouri batholith in Hildenbrand and Hendricks (1995). Another prominent low Vs anomaly is present on the Arkansas-Oklahoma border (labeled M in the 20 km slice of the map view). This low Vs area corresponds to the Arkoma Basin and is also imaged in the Geng et al. (2020) study. A prominent low-velocity region (labeled N in the map view) is present in Alabama and middle Tennessee, which agrees with Geng et al. (2020). Biryol et al. (2016) hypothesized that this area is underlain by thinned lithosphere. The lithospheric foundering might have caused heating and chemical differentiation, which explains the generation of silica-rich magmas and thus the observed low velocity. Low velocities at 60-150 km (labeled O) below the Mississippi Embayment with high velocities above (labeled I in the map view) agree with previous mantle velocity studies (Geng et al., 2020; Nyamwandha et al., 2016), and are similar to velocity anomalies below the North China Craton (Santosh et al., 2010; Tian & Zhao, 2011). Two slow anomalous regions in the uppermost mantle are present below the WVSZ and the SGSZ (labeled Q and R in cross-sections DD' and EE'), which are also present in the study by Geng et al. (2020).

Our study differs from the shear velocity model by Chen et al. (2016) in that low crustal Vs is imaged below the southern Illinois Basin (labeled L in the 24 km and 36 km slices of the map view); in the study by Chen et al. (2016), this area is characterized by high crustal Vs. The high crustal velocities are interpreted as mafic intrusions related to Paleozoic rift development; mafic materials extracted from the mantle may have entered the lower crust and increased the density and seismic velocity (Braile et al., 1986; Keller et al., 1983; Mooney et al., 1983). The presence of low crustal velocities below the southern Illinois Basin in our model contradicts the

426 interpretation by Chen et al. (2016), and thus does not support the idea that the southern Illinois
427 Basin has a rift origin. While a lot of evidence (e.g., Braile et al., 1986; Kolata and Nelson, 1991,
428 1997; Marshak and Paulsen, 1996) indicates that rifting influenced the Phanerozoic evolution of
429 the Illinois Basin, rifting may not be the initial mechanism that formed the basin (Bedle & van
430 der Lee, 2006).

431 5.1 Rayleigh wave phase velocities

432 The Rayleigh wave phase velocity images obtained in our study agree in general with the
433 previous study by Chen et al. (2016). Fundamental mode Rayleigh wave phase velocity maps
434 were determined using TA and OIINK stations in the Chen et al. (2016) study. The station
435 density in the center of our study area is improved compared to the station density in Chen et al.
436 (2016), and our study area is extended southward to 35°N because we include NELE stations. As
437 a consequence, our phase velocity maps revealed some features that are not found in the Chen et
438 al. (2016) study. For example, although high velocities underneath the upper ME (labeled A in
439 Figure 7) at the 20s period are found in both studies, these velocities also extend to the WVSZ
440 and the SGSZ in our model. We also observed features that extend anomalies imaged by Chen et
441 al. (2016) south of 35°N. These include a prominent low-velocity region corresponding to the
442 OAT-OR (labeled B) at 20 to 30s periods and low velocities in the southern ME (labeled D) in
443 the 50, 60, and 75s period maps.

444 Several features in our phase velocity maps are consistent through multiple periods. The
445 RR is characterized by average to low velocities (labeled D) and is flanked by high-velocity
446 regions. This pattern is apparent not only at 30s, but also at 40-100s periods. The presence of low
447 velocities is associated with the tectonic history of the RR, which involves the intrusive activity
448 related to the passage of the Bermuda hotspot in the Cretaceous (Cox & Van Arsdale, 1997), and

449 the thinning of the lithosphere during the early Cambrian rifting of supercontinent Rodina (Cox
450 & Van Arsdale, 2002). Slow velocities in the upper mantle are also attributed to the presence of a
451 subducted slab, as discussed below. The flanking high-velocity regions on both sides of the RR
452 are interpreted as either intact or foundering pieces of the old continental lithosphere (Biryol et
453 al., 2016; Nyamwandha et al., 2016). Another feature consistent throughout multiple periods is
454 the high velocities below the Illinois Basin (labeled G) and the surrounding low velocities
455 (labeled F and H). This high and low velocity pattern is apparent at 90 and 100s periods and is
456 also suggested in the 75s phase velocity map.

457 The low phase velocities associated with the OAT-OR coincide with the location of the
458 Arkoma Basin that formed by crustal loading during the Ouachita orogeny (Thomas, 1991). The
459 origin requires variations in the flexural rigidity of the crust and cannot be explained by basin fill
460 alone. As a result of the transition from the rift to the transform fault, thicker crust with lower
461 flexural rigidity occurs in the eastern portion of the basin and thinner crust with higher rigidity
462 occurs in the western portion of the basin (Harry & Mickus, 1998). The gravity anomaly is partly
463 due to the presence of thick syn-rift sediment accumulated at the OAT-OR intersection (Kruger
464 & Keller, 1986), which is commonly found along transform boundaries (e.g., Thomas, 2014).
465 The presence of low phase velocities at periods 20-30s in our study supports the concept that
466 basement structure is a contributing factor to the observed gravity anomaly.

467 5.2 Implications for the origin of the Illinois Basin

468 Theories regarding the origin of the Illinois Basin remain controversial. Chen et al.
469 (2016) find high Vs in the mid and lower crust below the southernmost part of the basin and
470 support the idea that basin formation is tied to formation of the Reelfoot Rift. McBride et al.
471 (2003) propose that the presence of a collapsed Proterozoic rhyolitic caldera complex or rift

below the central Illinois Basin is related to the formation of the Granite-Rhyolite basement and early formation of the basin. This would suggest that the Basin is considerably older than the Late Cambrian Reelfoot Rift. We observe low crustal Vs in the central part of the Illinois Basin (labeled K in the 24 km and 36 km slices of the map view Figure 8), which agrees with the Chen et al. (2016) study. The lack of high Vs at mid-crustal depths was used by Chen et al. (2016) to argue against the caldera/rift interpretation because a large mafic underplated layer is not present, as is the case for some ~1.4 Ga granites in the southwest U.S. (Snelson et al., 2005). McBride et al. (2003) suggest that the igneous activity did not involve the lower crust or mantle and thus, a mafic layer did not form. Our results tend to favor an origin for the Illinois Basin that is not directly associated with the same rifting event that formed the Reelfoot Rift. Unlike the study by Chen et al. (2016), we do not find high Vs in the depth range 24 to 36 km in the southern portion of the basin. We suggest that alternate explanations for formation of the basin, such as tectonic events associated with formation of the Granite-Rhyolite Provence, be considered in future studies.

5.3 LVZs below the mid-continent of North America

The presence of two anomalously slow regions extending from ~200 to 400 km forming a northwest dipping low-velocity zone (LVZ) below the Illinois Basin were detected in a recent study by Geng et al. (2020). Synthetic models indicate that the LVZ is connected to the low-velocity anomaly below the Reelfoot Rift imaged in previous studies (e.g., Bedle & van der Lee, 2006; Chen et al., 2016; Nyamwandha et al., 2016; Pollitz & Mooney, 2014). Anomaly O in our Vs model (Figures 8 and 9) is the upper portion of the LVZs observed in Nyamwandha et al. (2016) and Geng et al. (2020). The anomalously slow regions in the mantle underneath the Mississippi Embayment and the Illinois Basin are produced by fluids rising from a stalled slab

(Sigloch, 2011; Sigloch et al., 2008), according to the analysis in these previous studies. Calculations show that the saturation of water, temperature elevation, and the enrichment of orthopyroxene (opx) and iron content are required to explain the reduced seismic velocities in the mantle (Geng et al., 2020; Saxena, 2020; Saxena et al., 2017). Metasomatism of mantle rocks due to the ascending silica-rich fluids from the transition zone is the likely source of the opx enrichment. Silica from subducted ocean crust and sediment is transported into the overlying mantle during the dehydration process (Kusky et al., 2014; Wagner et al., 2008). The LVZs are closely related to the presence of the Hess plateau conjugate, a thick portion of the Farallon plate that is located below the CUS at transition zone depths (Liu et al., 2008; 2010). Our results suggest that the LVZ extends to near Moho depths below the Reelfoot Rift (Figure 9) and the Appalachian Basin.

5.4 Implications for the origin of intraplate seismicity

Correlations between the locations of low mantle velocities and intraplate seismic zones indicate that seismic velocities in the mantle contribute to the occurrence of intraplate earthquakes. The two low Vs anomalies in the upper mantle located below the WVSZ and the SGSZ (labeled Q and R in cross-sections DD’ and EE’, Figure 9) are probably weak zones with low shear strength embedded in a stronger lithosphere (Chen et al., 2014; Nyamwandha et al., 2016). Zhan et al. (2016) showed, using geodynamic modeling, that tectonic stresses concentrate in weak zones and will transfer to existing faults in the upper crust. The presence of these weak zones may play an essential role in the stress concentration of the intraplate seismic zones in the CEUS.

6 Conclusions

We developed a shear wave velocity model for the crust and upper mantle beneath the northern Mississippi Embayment and southern Illinois Basin by inverting the Rayleigh wave phase velocity data from Basu (2019). The low Vs zone detected in the mantle below the Reelfoot Rift is the upper portion of the LVZs imaged in Nyamwandha et al. (2016) and Geng et al. (2020). According to the analyses presented in these previous studies, the low velocities are produced by silica-rich fluids ascending from a trapped portion of the Farallon slab. Low crustal Vs is found in the central Illinois Basin, supporting the presence of a Proterozoic caldera related to the formation of the Granite-Rhyolite basement (McBride et al., 2013). Our model differs from the Chen et al. (2016) study in that the southern Illinois Basin is characterized by low Vs in the lower crust rather than high Vs, which does not support the concept that this portion of the Illinois Basin has a rift origin. Low-velocity zones below the WVSZ and the SGSZ suggest a connection between seismic velocities in the mantle and the occurrence of intraplate earthquakes. These low-velocity zones are regions with low shear strength and may be responsible for stress concentrations in the WVSZ and the SGSZ.

Data Availability Statement

The vertical component seismograms were acquired from the IRIS DMC facility (https://ds.iris.edu/ds/nodes/dmc). The starting models, Rayleigh wave phase velocities, and other essential datasets utilized in this study are available at https://data.mendeley.com/datasets/svxv8ytg9h/1 (doi: 10.17632/svxv8ytg9h.1).

Acknowledgment

We would like to thank Dr. Robert Herrmann at the Saint Louis University for developing the code for running shear velocity inversion and providing a 1-D Vs starting model. The permission for accessing NELE and OIINK datasets was authorized by the Center for Earthquake Research and Information at the University of Memphis.

References

Basu, U. (2019). *Seismic Velocity and Anisotropy Structure Underneath The Central United States* PhD Dissertation, The University of Memphis, Memphis, Tennessee, 102 pp.

Basu, U., & Powell, C. (2019). Pn tomography and anisotropy study of the central United States. *Journal of Geophysical Research: Solid Earth*, *124*(7), 7105-7119.

Bedle, H., & van der Lee, S. (2006). Fossil flat-slab subduction beneath the Illinois basin, USA. *Tectonophysics*, *424*(1-2), 53-68.

Bedle, H., & Van Der Lee, S. (2009). S velocity variations beneath North America. *Journal of Geophysical Research: Solid Earth*, *114*(B7).

Bickford, M., Van Schmus, W., Karlstrom, K., Mueller, P., & Kamenov, G. (2015). Mesoproterozoic-trans-Laurentian magmatism: A synthesis of continent-wide age distributions, new SIMS U–Pb ages, zircon saturation temperatures, and Hf and Nd isotopic compositions. *Precambrian Research*, *265*, 286-312.

555 Biryol, C. B., Wagner, L. S., Fischer, K. M., & Hawman, R. B. (2016). Relationship between
556 observed upper mantle structures and recent tectonic activity across the Southeastern
557 United States. *Journal of Geophysical Research: Solid Earth, 121*(5), 3393-3414.

558 Braile, L. W., Hinze, W. J., Keller, G. R., Lidiak, E. G., & Sexton, J. L. (1986). Tectonic
559 development of the New Madrid rift complex, Mississippi embayment, North America.
560 *Tectonophysics, 131*(1-2), 1-21.

561 Brazitis, D., & Conder, J. A. (2016). Microseismicity of the intraplate northern Wabash fault
562 system and La Salle Anticlinorium, Illinois Basin, USA. *Seismological Research Letters,*
563 *87*(6), 1479-1486.

564 Bristol, H. M., & Treworgy, J. D. (1979). The Wabash Valley fault system in southeastern
565 Illinois. *Circular no. 509*.

566 Buehler, J., & Shearer, P. (2017). Uppermost mantle seismic velocity structure beneath USArray.
567 *Journal of Geophysical Research: Solid Earth*, *122*(1), 436-448.

568 Catchings, R. (1999). Regional Vp, Vs, Vp/Vs, and Poisson's ratios across earthquake source
569 zones from Memphis, Tennessee, to St. Louis, Missouri. *Bulletin of the Seismological*
570 *Society of America*, *89*(6), 1591-1605.

571 Chen, C., Gilbert, H., Andronicos, C., Hamburger, M. W., Larson, T., Marshak, S., Pavlis, G. L.,
572 & Yang, X. (2016). Shear velocity structure beneath the central United States:
573 implications for the origin of the Illinois Basin and intraplate seismicity. *Geochemistry,*
574 *Geophysics, Geosystems*, *17*(3), 1020-1041.

Chen, C., Zhao, D., & Wu, S. (2014). Crust and upper mantle structure of the New Madrid Seismic Zone: Insight into intraplate earthquakes. *Physics of the Earth and Planetary Interiors, 230*, 1-14.

Cox, R. T., & Van Arsdale, R. B. (1997). Hotspot origin of the Mississippi embayment and its possible impact on contemporary seismicity. *Engineering Geology, 46*(3-4), 201-216.

Cox, R. T., & Van Arsdale, R. B. (2002). The Mississippi Embayment, North America: a first order continental structure generated by the Cretaceous superplume mantle event. *Journal of Geodynamics, 34*(2), 163-176.

Csontos, R., Van Arsdale, R., Cox, R., & Waldron, B. (2008). Reelfoot rift and its impact on Quaternary deformation in the central Mississippi River valley. *Geosphere, 4*(1), 145-158.

Fraser, G. S., Thompson, T. A., Olyphant, G. A., Furer, L., & Bennett, S. W. (1997). Geomorphic response to tectonically-induced ground deformation in the Wabash Valley. *Seismological Research Letters, 68*(4), 662-674.

Geng, Y., Powell, C. A., & Saxena, A. (2020). Joint local and teleseismic tomography in the central United States: exploring the mantle below the upper Mississippi Embayment and the Illinois Basin. *Journal of Geophysical Research: Solid Earth, 125*(10), e2020JB020625.

Godey, S., Snieder, R., Villaseñor, A., & Benz, H. M. (2003). Surface wave tomography of North America and the Caribbean using global and regional broad-band networks: phase velocity maps and limitations of ray theory. *Geophysical Journal International, 152*(3), 620-632.

Grana, J. P., & Richardson, R. M. (1996). Tectonic stress within the New Madrid seismic zone. *Journal of Geophysical Research: Solid Earth, 101*(B3), 5445-5458.

Harry, D. L., & Mickus, K. L. (1998). Gravity constraints on lithosphere flexure and the structure of the late Paleozoic Ouachita Orogen in Arkansas and Oklahoma, south central North America. *Tectonics, 17*(2), 187-202.

Herrmann, R. B. (2013). Computer programs in seismology: An evolving tool for instruction and research. *Seismological Research Letters, 84*(6), 1081-1088.

Hildenbrand, T. G., & Hendricks, J. D. (1995). *Geophysical setting of the Reelfoot rift and relations between rift structures and the New Madrid seismic zone* (2330-7102).

Johnston, A. C., & Schweig, E. S. (1996). The enigma of the New Madrid earthquakes of 1811–1812. *Annual Review of Earth and Planetary Sciences, 24*(1), 339-384.

Keller, G., Lidiak, E., Hinze, W., & Braile, L. (1983). The role of rifting in the tectonic development of the midcontinent, USA. In *Developments in Geotectonics* (Vol. 19, pp. 391-412). Elsevier.

Kenner, S. J., & Segall, P. (2000). A mechanical model for intraplate earthquakes: Application to the New Madrid seismic zone. *Science, 289*(5488), 2329-2332.

Kennett, B., & Engdahl, E. (1991). Traveltimes for global earthquake location and phase identification. *Geophysical Journal International, 105*(2), 429-465.

Kennett, B. L., Engdahl, E., & Buland, R. (1995). Constraints on seismic velocities in the Earth from traveltimes. *Geophysical Journal International, 122*(1), 108-124.

Kruger, J., & Keller, G. (1986). Interpretation of crustal structure from regional gravity anomalies, Ouachita Mountains area and adjacent Gulf Coastal Plain. *AAPG Bulletin, 70*(6), 667-689.

Kusky, T. M., Windley, B. F., Wang, L., Wang, Z., Li, X., & Zhu, P. (2014). Flat slab subduction, trench suction, and craton destruction: Comparison of the North China, Wyoming, and Brazilian cratons. *Tectonophysics, 630*, 208-221.

Liang, C., & Langston, C. A. (2009). Three-dimensional crustal structure of eastern North America extracted from ambient noise. *Journal of Geophysical Research: Solid Earth, 114*(B3).

Marshak, S., Domrois, S., Abert, C., Larson, T., Pavlis, G., Hamburger, M., Yang, X., Gilbert, H., & Chen, C. (2017). The basement revealed: tectonic insight from a digital elevation model of the Great Unconformity, USA cratonic platform. *Geology, 45*(5), 391-394.

Marshak, S., & Paulsen, T. (1996). Midcontinent US fault and fold zones: A legacy of Proterozoic intracratonic extensional tectonism? *Geology, 24*(2), 151-154.

McBride, J. H. (1997). Variable deep structure of a midcontinent fault and fold zone from seismic reflection: La Salle deformation belt, Illinois basin. *Geological Society of America Bulletin, 109*(11), 1502-1513.

McBride, J. H., Kolata, D. R., & Hildenbrand, T. G. (2003). Geophysical constraints on understanding the origin of the Illinois basin and its underlying crust. *Tectonophysics, 363*(1-2), 45-78.

McKeown, F. A., Hamilton, R. M., Diehl, S. F., & Glick, E. E. (1990). Diapiric origin of the Blytheville and Pascola arches in the Reelfoot rift, east-central United States: Relation to New Madrid seismicity. *Geology, 18*(11), 1158-1162.

Montagner, J. (1986). Regional three-dimensional structures using long-period surface waves. *Ann. Geophys, 4*(B3), 283-294.

Montagner, J.-P., & Kennett, B. (1996). How to reconcile body-wave and normal-mode reference earth models. *Geophysical Journal International, 125*(1), 229-248.

Mooney, W. D., Andrews, M., Ginzburg, A., Peters, D., & Hamilton, R. (1983). Crustal structure of the northern Mississippi embayment and a comparison with other continental rift zones. *Tectonophysics, 94*(1-4), 327-348.

Nyamwandha, C. A., & Powell, C. A. (2016). Seismic anisotropy beneath the Mississippi Embayment and the New Madrid Seismic Zone: A study of shear wave splitting. *Journal of Geophysical Research: Solid Earth, 121*(11), 8239-8253.

Nyamwandha, C. A., Powell, C. A., & Langston, C. A. (2016). A joint local and teleseismic tomography study of the Mississippi Embayment and New Madrid Seismic Zone. *Journal of Geophysical Research: Solid Earth, 121*(5), 3570-3585.

Obermeier, S. (1998). Liquefaction evidence for strong earthquakes of Holocene and latest Pleistocene ages in the states of Indiana and Illinois, USA. *Engineering Geology, 50*(3-4), 227-254.

Okure, M. S., & McBride, J. H. (2006). Deep seismic reflectivity beneath an intracratonic basin: Insights into the behavior of the uppermost mantle beneath the Illinois basin. *Precambrian Research, 149*(3-4), 99-125.

Pollitz, F. F., Kellogg, L., & Bürgmann, R. (2001). Sinking mafic body in a reactivated lower crust: a mechanism for stress concentration at the New Madrid seismic zone. *Bulletin of the Seismological Society of America, 91*(6), 1882-1897.

Pollitz, F. F., & Mooney, W. D. (2014). Seismic structure of the Central US crust and shallow upper mantle: Uniqueness of the Reelfoot Rift. *Earth and Planetary Science Letters, 402*, 157-166.

Porritt, R. W., Allen, R. M., & Pollitz, F. F. (2014). Seismic imaging east of the Rocky Mountains with USArray. *Earth and Planetary Science Letters, 402*, 16-25.

Santosh, M., Zhao, D., & Kusky, T. (2010). Mantle dynamics of the Paleoproterozoic North China Craton: a perspective based on seismic tomography. *Journal of Geodynamics, 49*(1), 39-53.

Satô, Y. (1958). Attenuation, dispersion, and the wave guide of the G wave. *Bulletin of the Seismological Society of America, 48*(3), 231-251.

Saxena, A. (2020). *Investigating Intraplate Seismicity in the Central and Eastern US: Linking Observations and Numerical Models* (Doctoral dissertation, The University of Memphis).

Saxena, A., Choi, E., & Powell, C. A. (2017). Stress concentration on Intraplate Seismicity: Numerical Modeling of Slab-released Fluids in the New Madrid Seismic Zone. In *AGU Fall Meeting Abstracts* (Vol. 2017, pp. T54A-05).

Shen, W., & Ritzwoller, M. H. (2016). Crustal and uppermost mantle structure beneath the United States. *Journal of Geophysical Research: Solid Earth, 121*(6), 4306-4342.

679 Shen, W., Ritzwoller, M. H., & Schulte-Pelkum, V. (2013). Crustal and uppermost mantle
680 structure in the central US encompassing the Midcontinent Rift. *Journal of Geophysical*
681 *Research: Solid Earth, 118*(8), 4325-4344.

682 Sigloch, K. (2011). Mantle provinces under North America from multifrequency P wave
683 tomography. *Geochemistry, Geophysics, Geosystems, 12*(2).

684 Sigloch, K., McQuarrie, N., & Nolet, G. (2008). Two-stage subduction history under North
685 America inferred from multiple-frequency tomography. *Nature Geoscience, 1*(7), 458-
686 462.

687 Snelson, C. M., Keller, G. R., Miller, K. C., Rumpel, H.-M., & Prodehl, C. (2005). Regional
688 crustal structure derived from the CD-ROM 99 seismic refraction/wide-angle reflection
689 profile: The lower crust and upper mantle. *Washington DC American Geophysical Union*
690 *Geophysical Monograph Series, 154*, 271-291.

691 Tarantola, A., & Valette, B. (1982). Generalized nonlinear inverse problems solved using the
692 least squares criterion. *Reviews of Geophysics, 20*(2), 219-232.

693 Tavakoli, B., Pezeshk, S., & Cox, R. T. (2010). Seismicity of the New Madrid seismic zone
694 derived from a deep-seated strike-slip fault. *Bulletin of the Seismological Society of*
695 *America, 100*(4), 1646-1658.

696 Thomas, W. A. (1991). The Appalachian-Ouachita rifted margin of southeastern North America.
697 *Geological Society of America Bulletin, 103*(3), 415-431.

698 Thomas, W. A. (2014). A mechanism for tectonic inheritance at transform faults of the Iapetan
699 margin of Laurentia. *Geoscience Canada*, 321-344.

Thomas, W. A., & Powell, C. A. (2017). Necessary conditions for intraplate seismic zones in North America. *Tectonics, 36*(12), 2903-2917.

Thybo, H., Perchuć, E., & Zhou, S. (2000). Intraplate earthquakes and a seismically defined lateral transition in the upper mantle. *Geophysical research letters, 27*(23), 3953-3956.

Tian, Y., & Zhao, D. (2011). Destruction mechanism of the North China Craton: insight from P and S wave mantle tomography. *Journal of Asian Earth Sciences, 42*(6), 1132-1145.

Van der Lee, S. (2002). High-resolution estimates of lithospheric thickness from Missouri to Massachusetts, USA. *Earth and Planetary Science Letters, 203*(1), 15-23.

Van Der Lee, S., & Frederiksen, A. (2005). Surface wave tomography applied to the North American upper mantle. *Seismic Earth: Array analysis of broadband seismograms, 157*, 67-80.

Van der Lee, S., & Nolet, G. (1997). Upper mantle S velocity structure of North America. *Journal of Geophysical Research: Solid Earth, 102*(B10), 22815-22838.

Wagner, L. S., Anderson, M. L., Jackson, J. M., Beck, S. L., & Zandt, G. (2008). Seismic evidence for orthopyroxene enrichment in the continental lithosphere. *Geology, 36*(12), 935-938.

Whitmeyer, S. J., & Karlstrom, K. E. (2007). Tectonic model for the Proterozoic growth of North America. *Geosphere, 3*(4), 220-259.

Yang, X., Pavlis, G. L., Hamburger, M. W., Marshak, S., Gilbert, H., Rupp, J., Larson, T. H., Chen, C., & Carpenter, N. S. (2017). Detailed crustal thickness variations beneath the Illinois Basin area: Implications for crustal evolution of the midcontinent. *Journal of Geophysical Research: Solid Earth, 122*(8), 6323-6345.

722 Yang, X., Pavlis, G. L., Hamburger, M. W., Sherrill, E., Gilbert, H., Marshak, S., Rupp, J., &
723 Larson, T. H. (2014). Seismicity of the Ste. Genevieve seismic zone based on
724 observations from the EarthScope OIINK flexible array. *Seismological Research Letters, 85*(6), 1285-1294.

726 Yao, H., Van Der Hilst, R. D., & Montagner, J. P. (2010). Heterogeneity and anisotropy of the
727 lithosphere of SE Tibet from surface wave array tomography. *Journal of Geophysical*
728 *Research: Solid Earth, 115*(B12).

729 Zhan, Y., Hou, G., Kusky, T., & Gregg, P. M. (2016). Stress development in heterogenetic
730 lithosphere: Insights into earthquake processes in the New Madrid Seismic Zone.
731 *Tectonophysics, 671*, 56-62.

732 Zhang, Q., Sandvol, E., & Liu, M. (2009). Tomographic Pn velocity and anisotropy structure in
733 the central and eastern United States. *Bulletin of the Seismological Society of America, 99*(1), 422-427.

735

736 Figure 1. 348 NELE, CERI, OIINK, and TA stations utilized in the Basu (2019) study to obtain
737 Rayleigh wave phase velocities. SS, the Sparta Shelf; OD, the Ozark Dome; ND, the Nashville
738 Dome; OAT, the Oklahoma-Alabama Transform; OR, the Ouachita Rift; NMSZ, the New
739 Madrid Seismic Zone; SGSZ, the Ste. Genevieve Seismic Zone; WVSZ, the Wabash Valley
740 Seismic Zone. A dashed line in dark red represents the Nd line. Fault traces and fold systems are
741 delineated with green solid lines and white solid lines, respectively. Boundaries of the Illinois
742 Basin, the Mississippi Embayment, and the Reelfoot Rift are marked with dashed lines in blue,

743 black, and purple, respectively. Grid nodes used to present the phase velocity maps by Basu
744 (2019) are denoted with empty dots.

745

746 Figure 2. The azimuthal distribution and ray paths of 104 regional and teleseismic events with
747 magnitudes ≥5.0 and epicentral distances 5°-120° (measured from the center of the northern
748 Mississippi Embayment), from Basu (2019). They were selected over a period of five years
749 (from 2011 to 2015).

750

751 Figure 3. Averaged dispersion curve of Rayleigh wave phase velocities measured by combining
752 data from all the grid nodes. The lengths of the blue bars are proportional to the magnitudes of
753 standard errors.

754

755 Figure 4. Starting models used to test the stability of shear velocity inversion: (a), the Herrmann
756 (2013) model with variations of crustal or mantle velocities of ±0.2 km/s; (b), the Chen et al.
757 (2016) model with variations of crustal or mantle velocities of ±0.2 km/s.

758

759 Figure 5. Impact of the starting model on the resultant Vs profile at (38.25°N, 90.50°W): (a) the
760 dispersion curve used to invert for Vs structure; (b) velocities resolved using the Herrmann
761 (2013) model with variations of crustal or mantle velocities; (c) velocities resolved using the
762 Chen et al. (2016) model with variations of crustal or mantle velocities.

763

764 Figure 6. Impact of the starting model on the resultant Vs profile at (38.25°N, 88.00°W): (a) the
765 dispersion curve used to invert for Vs structure; (b) velocities resolved using the Herrmann
766 (2013) model with variations of crustal or mantle velocities; (c) velocities resolved using the
767 Chen et al. (2016) model with variations of crustal or mantle velocities.

768

769 Figure 7. Isotropic phase velocity maps from simultaneous inversion for 20-100s periods. Fault
770 traces and fold systems are delineated with solid green lines and solid gray lines, respectively.
771 The Ozark Dome and the Nashville Dome are delineated with an orange circle and a dark red
772 circle, respectively. A purple dashed line marks the boundary of the Reelfoot Rift. The
773 boundaries of the Illinois Basin and the Mississippi Embayment are delineated with a blue
774 dashed line and a black dashed line, respectively.

775

776 Figure 8. Horizontal slices of the 3-D Vs model created by joining all the 1-D profiles. Crustal
777 velocities and mantle velocities are presented using different color scales. Major geology
778 features are labeled with the same notations as those in Figure 7.

779

780 Figure 9. Vertical slices of the 3-D Vs model. The 4.2 km/s velocity contour is used to represent
781 the Moho. Notations for major geology features: BA, the Blytheville Arch; OD, the Ozark
782 Dome; SS, the Sparta Shelf; PA, the Pascola Arch; App, the Appalachian Mountains; NMSZ, the
783 New Madrid Seismic Zone; SGSZ, the Ste. Genevieve Seismic Zone; WVSZ, the Wabash Valley
784 Seismic Zone. On the map view, the blue circle and the red circle mark the boundaries of the

785 Sparta Shelf and the Ozark Dome, respectively; dashed rectangles mark the locations of
786 intraplate seismic zones; fault zones are delineated with thick, orange lines.

787

788 Table 1. Rayleigh wave phase velocities between 20 sec and 100 sec measured by combining
789 data from all the grid nodes.

790